

# An MTF Analysis of Landsat Classification Error at Field Boundaries

Jess Grunblatt

Ministry of Planning and National Development, Kenya Rangeland Ecological Monitoring Unit, Nairobi, Kenya

**ABSTRACT:** The purpose of this study was to evaluate image classification error as affected by the performance characteristics of the Landsat multispectral scanner (MSS). The MSS modulation transfer function (MTF) was chosen as a means of defining the ability of the MSS sensor to transfer spectral variations in the intensity of reflected radiation (modulation), received at the satellite sensor, to the image data. The MSS MTF was used to predict the degradation of image quality (blur) at field boundaries. A study area of large, homogeneous, agricultural fields of various crop types was selected from a Landsat-2 image and classified. Classification error at field boundaries was compared to the boundary blur predicted by the MSS MTF analysis. A postclassification algorithm employing field boundary information was used to minimize boundary blur impacts on classification accuracy.

## BACKGROUND

THE SUCCESS of image classification studies is generally evaluated according to the percentage error of the final results. Such evaluations are specific to the method of analysis used to extract information from a particular image for a specific application problem. Another way to evaluate image classification is to define the smallest object of interest and to use spatial frequency analysis to determine how that object is recorded by the sensor (Brock, 1970). Slater (1973) suggests just this approach in evaluating the Landsat system. By computation of the multispectral scanner (MSS) modulation transfer function (MTF), he suggested that researchers could define relationships between the quantity and quality of Earth resource data that could be extracted from the imagery.

The MTF is a measure of sensor performance that describes the ability of a sensor to transfer modulation from viewed objects to image data. The MTF can be used to determine the image that would be produced by a given sensor. The use of the MTF requires the transformation of a scene into its frequency spectrum; that is, the radiance profile of a scene must be described as a function of spatial frequency rather than as a function of distance.

A sensor's ability to transfer modulation can also be analyzed in terms of the distance or space domain by using the system point spread function (PSF). The PSF is the inverse Fourier transform of the MTF. It describes the spreading within the recorded image of an infinitely small object point source. Similarly, a line spread function (LSF) considers sensor performance relative to an isolated source of radiance infinitely small in one dimension and infinitely long in another. By convolving this LSF with an edge, we obtain the edge spread function (ESF). The ESF defines the extent to which a discrete object boundary or edge is spread or blurred by an imaging system. The ESF indicates both the distance and magnitude of boundary blur.

Figure 1 illustrates the significance of instantaneous field-of-view (IFOV) in determining the quality of image data. If two small objects are separated by a distance less than the IFOV of the sensor, the radiance value recorded for these objects will be an average of the radiance from all materials within the IFOV of the sensor. Similarly, when the IFOV overlaps discrete object boundaries, radiance contributions from both objects will determine the recorded radiance value.

In 1973 a NASA working group and Slater (1973) suggested a measure of system performance that could relate the MTF to spatial terms. The effective instantaneous field-of-view (EIFOV) was proposed: i.e.,

$$\text{EIFOV} = 1/U_c$$

where  $U_c$  is the effective system cutoff frequency, i.e., the spa-

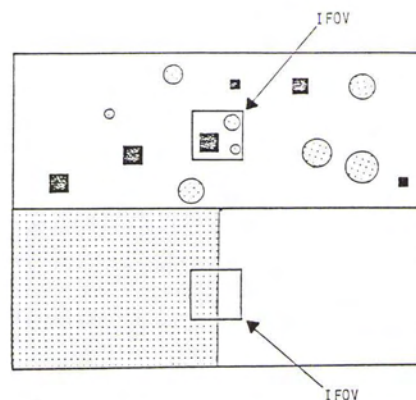


FIG. 1. Relationships between IFOV and object size that inhibit modulation transfer by sensor from object scene to image data.

tial frequency (cycles/m) at which the MTF is reduced to 0.5. This value corresponds to the LSF or ESF width at half maximum.

Both IFOV and EIFOV are descriptive of the minimum scene area that contributes to a single digital measurement by the MSS. Unlike the IFOV, which is determined by the fiber optics of the sensor, EIFOV can reflect whatever components are considered in the MTF analysis. The performance characteristics of the optical, detector, and electronic subsystems of the sensor as well as such factors as atmospheric effects, data resampling algorithms, and data sampling within the sensor affect the transfer of modulation from the object scene to the image data.

Markham (1985) calculated a presampled nadir EIFOV for the MSS as 79 to 82 m along-scan and 70 to 75 m along-track. These calculations considered the capabilities of the optical, detector, and electronic components of the sensor in modulation transfer. Park *et al.* (1984) presented a stochastic approach to MSS MTF analysis that considered sensor sampling interval and bilinear resampling contributions to MTF as well as the performance of the sensor components. This evaluation of the MSS sensor components determined a 77 m scan by 65 m track EIFOV based on 63 m by 63 m EIFOV for the scanning aperture. The effect of sampling was estimated to increase the EIFOV 9 m in the along-scan direction and 57 m in the along-track direction. Bilinear resampling of the data produced an additional increase of 18 m in the along-scan and 26 m in the along-track directions. An overall EIFOV of 104 m scan by 148 m track was thus determined.

The impacts of modulation loss at a boundary are illustrated in the following example. Figure 2 represents a hypothetical ESF. The values indicated by this curve correspond to the percent contrast between adjacent objects detected by the sensor

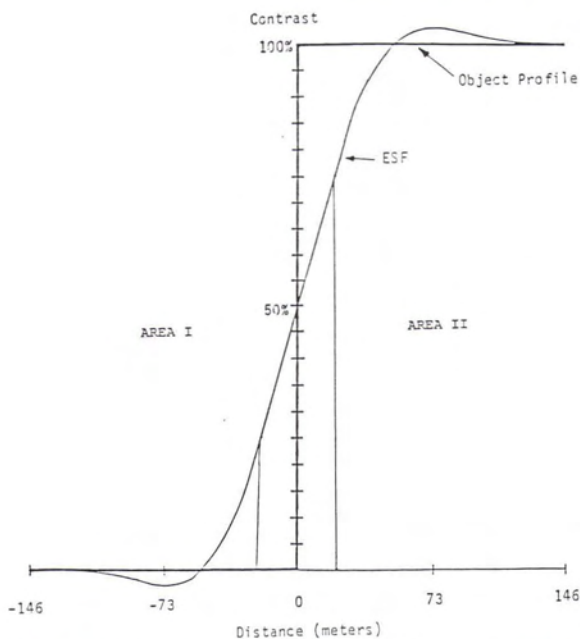


FIG. 2. ESF with sampling interval at  $\pm 29$  m, illustrating boundary blur.

as the sensor scans across the boundary between two objects. The ESF is the analog data stream of an edge as would be monitored by the sensor. In this example the distance from the boundary where the ESF is the correct object radiance level occurs at a distance of 58 m from the boundary. A sampling interval at  $\pm 29$  m is illustrated in this example. Assuming a pixel size of 58 m in this sampling phase, boundary blur will have a major impact on the detected radiance level as 20 percent of the boundary contrast is added to the AREA I pixel value and 20 percent of the contrast is subtracted from the AREA II value. However, the location of the boundary is accurately portrayed. If the sampling interval should occur at other than the  $\pm 29$  m interval, then, in addition to the reduction in radiance level of the boundary pixel, the boundary will also be spatially misrepresented in the image data.

The significance of modulation loss at a boundary relative to image classification can be most easily understood by examining an ellipse plot that represents a two-dimensional hypothetical data set (Figure 3). A two-class example can be defined by means  $Q$  and  $Z$  and their associated variances. The distance between means is represented by vector  $\overline{QZ}$ .

The impact of the boundary blur is to create an artificial class of boundary pixels whose radiance values are distributed between the radiance values of the adjacent classes. Therefore, these boundary pixels can occur anywhere along vector  $\overline{QZ}$ . Generally, the probability of class occurrence in maximum likelihood classifiers is inversely proportional to the statistical distance between a point and a class category, assuming *a priori* probabilities are equal. Therefore, these boundary pixels will be classified as either  $Q$  or  $Z$ , depending on the extent of the boundary blur on these pixels as determined by the sampling interval.

Figure 3 also illustrates a three-class example where a third class,  $Y$ , lies between  $Q$  and  $Z$ . Most boundary errors will now be contained by class  $Y$ , and therefore, at an edge between  $Q$  and  $Z$ , one would expect to find pixels erroneously classified as class  $Y$ .

A variety of methods have been used to reconstruct boundary pixels to enhance classification accuracy (Metzler, 1983; Nalepka *et al.*, 1971). A postprocessing algorithm incorporating object boundary information was examined in this analysis to reduce classification error due to modulation loss at object boundaries. As the boundary information used in this analysis was derived

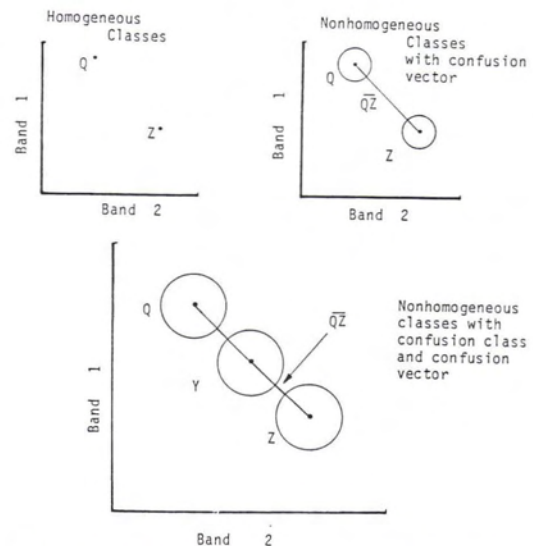


FIG. 3. Hypothetical ellipse plots of spectral signatures, illustrating classification confusion produced by boundary blur.



FIG. 4. Landsat-2 RBV image of the Orchard Quadrangle Study Area. The large center pivot irrigation systems are generally 395 hectares (160 acres) in size.

from standard remote sensing products, the postprocessing method offered in this analysis provides a simple correction for areas of large homogeneous objects.

## METHODS

The classification analysis was conducted through the cooperation of the Colorado State University (CSU) Extension Service, CSU Experiment Station, and the Colorado State Forest Service under NASA contract NAS5-25081. A complete description of the classification methods can be found in Maxwell *et al.* (1980).

An area within the Orchard topographic quadrangle, Morgan County, near Greeley, Colorado, was chosen as the classification study area. Figure 4 shows a portion of the Landsat return beam

vidicon (RBV) image for the Orchard Study Area. This region is dominated by center pivot irrigation systems, largely quarter section (395 hectares or 160 acres) in size. It is, therefore, a good approximation of the desired model of large homogeneous fields with discrete boundaries. Crop identities within a continuous region in this area were determined by field crews. This study site contained 2257 pixels of corn, 419 pixels of sugar beets, 357 pixels of hay, 531 pixels of beans, and 164 pixels of rangeland/uncultivated. On the basis of a seasonal signature analysis, the 16 August 1978 image date was selected as an optimal date for discrimination of the crop types in this area.

All Landsat data were geometrically corrected using nearest neighbor resampling (76-m by 58-m pixels). The image data selected for analysis had no evidence of striping.

Field boundaries for the study area were determined from RBV imagery of approximately 1:125,000 scale and from 1:24,000 United States Geological Survey orthophoto quadrangle maps. The Landsat RBV was used to update the orthophoto information. Aerial photographs of 1:8000 scale were used to verify the field boundaries.

Signatures used in classification were developed according to a "modified unsupervised" method. The area of interest was input to an iterative clustering routine to determine the general spectral composition of the area. These unsupervised clusters were compared with data sets acquired from other agricultural areas to determine groupings of spectral interest. From areas of spatial regularity, rectangles and circles, supervised samples were extracted. Mean, standard deviation, skewness, and kurtosis values were evaluated to ensure field center pixels were used in the analysis. Probable crop identities were chosen for data sets based on signatures developed in the analysis of other similar agricultural districts. These training sets were used in a maximum likelihood algorithm for the classification of the Orchard Study Area.

Field classification accuracy within the Orchard Study Area was then evaluated as a function of distance from the field boundary. This was accomplished by placing concentric rings inside the field boundaries at a distance of one- and two-pixel widths (Figure 5). The classified identity of each pixel within these concentric rings was recorded as was the actual identity of the pixel.

Field boundary information was used in a postprocessing reclassification of the data once boundary error had been established. Pixel identity was reassigned according to the majority class occurrence within the field.

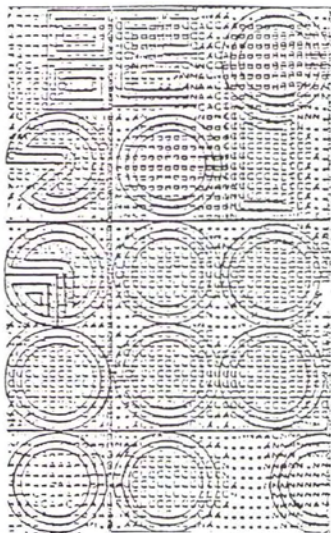


FIG. 5. Fields with concentric rings placed at one- and two-pixel widths from the field boundary.

## CLASSIFICATION RESULTS AND DISCUSSION

Classification results were evaluated for the entire field, after excluding ring one and after excluding rings one and two. The errors in classification associated with ring one, ring two, and the interior portion of the field were determined. These results are summarized in Table 1 and Figure 6.

Overall recognition of the corn and beets is 70 to 80 percent. Approximately 40 percent error is associated with the first pixel ring position in these fields. Error rapidly drops to 15 to 20 percent for the second pixel and high recognition, 0 to 5 percent, is noted for the interior pixels.

The poor recognition of hay was expected on this image date because the fall cutting of hay was occurring. Therefore, hay existed in conditions ranging from uncut, to freshly cut, to partially regrown. High errors for this class were expected and are indicated in Table 1. Two fields exhibited almost complete misclassification. Removal of these fields from the data set produced curve Hay2 in Figure 6.

Bean fields at the date of the image were being prepared for an early September harvest (Knott, personal communication, 1980). This required the cessation of irrigation around the middle of August to allow the fields to dry. The onset of chlorosis resulted in a highly varied spectral signature for beans at this

TABLE 1. CLASSIFICATION RESULTS FOR ORCHARD QUADRANGLE STUDY AREA FOR ZERO-, ONE-, AND TWO-PIXEL WIDTHS FROM FIELD BORDER

	Total Classification					
	Corn	Beets	Hay	Beans	Range	% Correct
Corn	1754	73	183	179	68	77.7
Beets	27	345	4	41	2	82.3
Hay	27	103	119	71	37	33.3
Beans	47	13	238	238	41	44.8
Range	3	2	41	23	95	57.9

	Classification Excluding Ring 1					
	Corn	Beets	Hay	Beans	Range	% Correct
Corn	1286	28	58	53	9	89.7
Beets	2	249	0	8	0	96.1
Hay	5	63	88	22	9	47.1
Beans	32	10	142	163	17	44.8
Range	0	0	18	6	75	75.8

	Classification Excluding Rings 1 & 2					
	Corn	Beets	Hay	Beans	Range	% Correct
Corn	807	12	19	3	1	95.8
Beets	0	147	0	1	0	99.3
Hay	3	22	52	8	2	59.8
Beans	22	9	98	92	7	40.9
Range	0	0	5	1	32	89.2

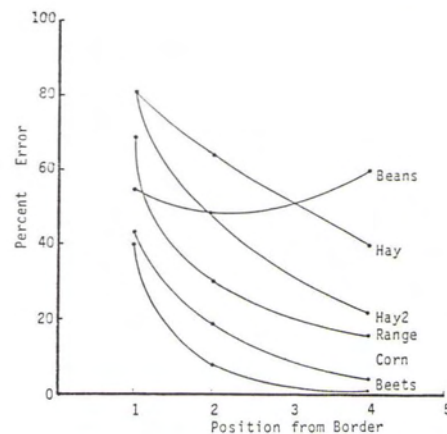


FIG. 6. Percentage classification error as a function of distance from field border.

image date. High error is noted for both boundary as well as field center pixels (Figure 6).

The range category used in this analysis represents a wide variety of uncultivated land-cover types. Overall accuracy of 58 percent is noted. By excluding ring 1 pixels from the analysis, an accuracy of 76 percent was achieved. Removal of the ring 1 and 2 pixels resulted in an accuracy of 89 percent.

Figure 7 contains a plot of the percent classification error normalized for residual interior error. From this we see that the first pixel errors ranged from 40 to 60 percent and second pixel error ranged from 8 to 25 percent.

The EIFOV determined by Park *et al.* (1984) suggests that significant modulation degradation of second position pixels would occur. The second pixels error noted in this classification analysis appears consistent with those conclusions.

Several contributors to boundary classification error relevant to this analysis, in addition to those present in Park *et al.* (1984), should also be considered. The MTF analysis presented earlier assumes an ideal edge. Transition at such a boundary occurs instantaneously from one area to another. In actuality, field boundaries are far from ideal. Natural edges vary in extent from narrow fence rows to boundaries that include fences, hedgerows, roads, irrigation ditches, etc. A natural boundary frequently corresponds to an area of unique reflectance characteristics and is not just a transition between two areas of different reflectance. In addition, nonorthogonal orientation of field boundaries relative to the scan direction and rectangular IFOV can also vary the radiance detected at a boundary. Finally, the modulation loss due to nearest neighbor resampling can be expected to be greater than that resulting from bilinear resampling (Schowengerdt, 1984).

In this analysis a postprocessing step was employed where field identity was reassigned according to the majority class occurrence within the field. Substantial improvement was noted in class recognition after post processing (Table 2). Field sizes less than 5 by 5 pixels cannot be expected to be accurately classified because such areas would be completely effected by boundary blur. Transition pixels determined by adjacent contrast and the sensor sampling interval would dominate for such areas.

## CONCLUSIONS

Investigation of the Landsat MSS EIFOV suggests significant modulation loss at a boundary. The magnitude of modulation loss observed at the boundary varies according to the contrast at the boundary; however, the proportion of that contribution relative to the total contrast at the boundary is consistent.

Modulation loss at a boundary—boundary blur—causes the formation of transition pixels. These transition pixels are not

TABLE 2. CLASSIFICATION RESULTS FOR ORCHARD QUADRANGLE STUDY AREA FOR RAW AND POSTPROCESSED CLASSIFICATION DATA

	Cultivated Fields and Range Without Post Processing					
	Corn	Beets	Alfalfa	Beans	Range	% Correct
Corn	1754	73	183	179	68	77.7
Beets	27	345	4	41	2	82.3
Alfalfa	27	103	119	71	37	33.3
Beans	47	13	238	238	41	44.8
Range	3	2	41	23	95	57.9

	Cultivated Fields and Range With Post Processing					
	Corn	Beets	Alfalfa	Beans	Range	% Correct
Corn	2226	0	24	0	0	99
Beets	0	419	0	0	0	100
Alfalfa	0	48	220	78	0	62
Beans	0	0	225	308	0	57
Range	0	0	42	0	122	74

indicative of a particular cover type but rather are descriptive of a mixture of adjacent cover types. The effect of these transition pixels on digital classification accuracy is a function of the magnitude of the boundary blur, the relative positions of class signatures in the spectral decision space, and average field size.

Investigation of boundary blur in an agricultural classification example indicated a 40 to 60 percent classification error in the pixels nearest the boundary and an 8 to 25 percent misclassification in the secondary pixel positions. The extension of classification error to secondary position pixels would be expected given an EIFOV of approximately twice the IFOV of the MSS, as indicated by Park *et al.* (1984). Such classification error underlines the impact of the data sampling within the MSS and of resampling algorithms used to manipulate MSS data on the quality of image data.

Additional sources of classification error could also include the presence of continuous transition areas that are more characteristic of natural boundaries than the discrete, instantaneous boundary assumed in the MTF analysis. Nonperpendicular boundaries relative to the direction of scan could also contribute to the secondary pixel error.

Modulation loss increases classification error at object boundaries due to boundary blur. Classification error within large areas, however, might be expected to decrease due to a reduction in detected object heterogeneity. Given adequate definition of spectral classes, the majority of pixels in a homogenous 5-by-5-pixel field should be correctly identified in MSS data. Provided adequate field boundary information exists, reassignment of field identity according to the majority class occurrence should substantially increase classification accuracy.

## ACKNOWLEDGMENT

The author would like to thank Dr. E.L. Maxwell, of the Solar Energy Research Institute, for valuable assistance during this research.

## REFERENCES

- Brock, G. C., 1970. *Image Evaluation for Aerial Photography*. The Focal Press, New York, New York. 258p.
- Markham, Brian L., 1985. The Landsat Sensor's Spatial Responses, *IEEE Transactions on Geoscience and Remote Sensing*, Vol. Ge-23, No. 6, pp. 864-875.
- Maxwell, E.L., R.M. Aherron, D. Fitz, G. Gross, J. Grunblatt, and A. Morse, 1980. *Monitoring Drought Impact from Landsat*. Final Report, Contract NAS5-25081, NASA/GSFC.
- Metzler, Michael D., and Richard C. Ciccone, 1983. Assessment of Technologies for Classification of Mixed Pixels. *Proceedings, Seventeenth International Symposium on Remote Sensing of the Environment*, Ann Arbor, Michigan.
- Nalepka, R. F., and P. D. Hyde, 1971. Classifying Unresolved Objects from Simulated Space Data, *Proceedings, Seventh International Sym-*

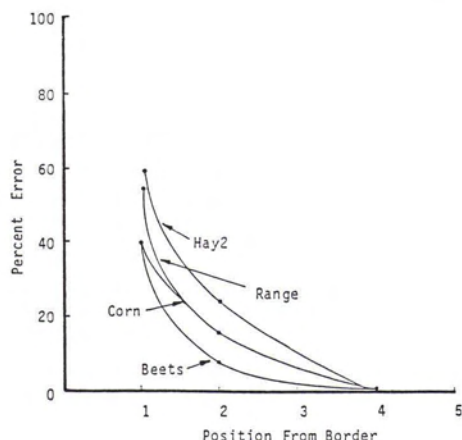


FIG. 7. Normalized percent classification error as a function of distance from field border.

- posium on Remote Sensing of the Environment*, Ann Arbor, Michigan. pp. 935-949.
- Park, S. K., Robert Schowengerdt, and Mary-Anne Kaczynski, 1984. Modulation Transfer Function Analysis for Sampled Image Systems, *Applied Optics*, Vol. 23, No. 15, pp. 2572-2582.
- Schowengerdt, R. A., Stephen K. Park, and Robert Gray, 1984. Topics in the Two-Dimensional Sampling and Reconstruction of Images, *Int. J. Remote Sensing*, Vol. 5, No. 2, pp. 333-347.
- Slater, P.N., and R. A. Schowengerdt, 1973. Sensor Performance for Earth Resources Studies, *Photogrammetric Engineering and Remote Sensing*, Vol. 39, No. 2, pp. 197-201.

Received 11 August 1986; revised and accepted 28 February 1987)

## Short Courses in Remote Sensing

The Australian Key Center in Land Information Studies  
University of Queensland

The Australian Key Center in Land Information Studies will be offering the following short courses in remote sensing:

- Introductory Courses
  - Introduction to Remote Sensing
  - Basic Digital Image Processing
- Sensor System Courses
  - SPOT
  - Aircraft MSS
  - Landsat TM
  - AVHRR
- Application Courses
  - Shallow Water Mapping
  - Geology
  - Arid Lands
  - Agriculture

For further information please contact

Miss Gail Kelly  
Course Co-ordinator for Remote Sensing  
Australian Key Centre for Land Information Studies  
University of Queensland  
St. Lucia, Queensland 4067  
Australia

## Forthcoming Articles

- Michael H. Brill, Triangulating from Optical and SAR Images Using Direct Linear Transformations.
- Henrik Haggren and Esa Leikas, Mapvision — The Photogrammetric Machine Vision System.
- Michael E. Hodgson, John R. Jensen, Halkard E. Mackey, Jr., and Malcolm C. Coulter, Remote Sensing of Wetland Habitat: A Wood Stork Example.
- Terrence Keating, William Phillips, and Kevin Ingram, An Integrated Topologic Database Design for Geographic Information Systems.
- William M. Kovalick, Jeffrey A. Newcomer, and Stephen W. Wharton, A Methodology for Evaluation of an Interactive Multispectral Image Processing System.
- James P. Ormsby and Ross S. Lunetta, Whitetail Deer Food Availability Maps from Thematic Mapper Data.
- Paul Ritter, A Vector-Based Slope and Aspect Generation Algorithm.
- Albert van Dijk, Susan L. Callis, Clarence M. Sakamoto, and Wayne L. Decker, Smoothing Vegetation Index Profiles: An Alternative Method for Reducing Radiometric Disturbance in NOAA/AVHRR Data.
- Stephen J. Walsh, Comparison of NOAA AVHRR Data to Meteorologic Drought Indices.